Evolution of Block Copolymer Lithography to Highly Ordered Square Arrays

Chuanbing Tang,[1] Erin M. Lennon,[1,2] Glenn H. Fredrickson,[1,2,3]* Edward J. Kramer,[1,2,3]* Craig J. Hawker[1,3,4]*

The manufacture of smaller, faster, more efficient microelectronic components is a major scientific and technological challenge, driven in part by a constant need for smaller lithographically defined features and patterns. Traditional self-assembling approaches based on block copolymer lithography spontaneously yield nanometer-sized hexagonal structures, but these features are not consistent with the industry-standard rectilinear coordinate system. We present a modular and hierarchical self-assembly strategy, combining supramolecular assembly of hydrogen-bonding units with controlled phase separation of diblock copolymers, for the generation of nanoscale square patterns. These square arrays will enable simplified addressability and circuit interconnection in integrated circuit manufacturing and nanotechnology.

One of the main limitations in the manufacture of integrated circuits is the difficulty in scaling the photolithographic techniques currently used during fabrication of complementary metal oxide semiconductor transistors to below 30 nm (*1*, *2*). One promising technique to achieve this scaling is block copolymer (BCP) lithography, which affords feature sizes that are dictated by the molecular weight of the block copolymer and are typically 10 to 30 nm (*3*–*8*). BCP lithography was recently used in the development of air-gap technology, in which hexagonal arrays of cylindrical pores are combined with photolithography to create multiple levels of porous dielectric nanostructures (*9*). Although BCP lithography is attractive because it can be done under simplified processing conditions with no requirement for expensive projection tools, a number of challenges exist (*10*). These include the development of strategies for producing a wide range of nanoscale patterns—for example, easily obtained hexagonal arrays as well as square arrays that are compatible with semiconductor integrated circuit design standards (*11*)—and of methods for controlling long-range order in the self-assembled BCP structures (*12*, *13*).

To address these challenges, we have focused on the fabrication of highly ordered square arrays of sub–20-nm features, without the need for an underlying square chemical pattern (*14*). For bulk materials, the traditional approach to preparing more complex self-assembled structures from block copolymers has been to progress from A-B diblock copolymers to more sophisticated A-B-C triblock copolymer systems. Multistep control of the precise composition of each segment of such A-B-C triblock copolymers, combined with the intricacies of controlling their thin-film morphologies, prompted our investigation into a simplified, modular approach to defining nanoscale features in polymeric thin films. In terms of modularity, simple blending of different diblock copolymers, such as A-B/B-C and A-B/C-D alloys, would seem to be attractive for combining physical properties and broadening the processing window (*15*–*17*). However, uniform long-range order has not been achieved in thin-film blends of block copolymers (*18*) because of the overwhelming tendency of such mixtures to exhibit macrophase separation (*19*–*22*).

In an attempt to limit macrophase separation in these blends, we have exploited supramolecular (H-bonding) interactions in addition to the nonspecific dispersive interactions typically present in a copolymer alloy (*23*, *24*). These attractive interactions between complementary H-bonding groups are designed to suppress macrophase separation in favor of microphase separation, thereby producing large-scale assembly of nanoscale features. By controlling the level of incorporation of H-bonding units, the molecular weights and compositions of the block copolymers, and the relative amounts of the two block copolymers in the alloy, a highly modular and tunable system can be developed that allows diverse families of ordered features to be achieved, including square arrays of cylinders.

The block copolymers were based on poly(ethylene oxide)-*b*-poly(styrene) (PEO-*b*-PS) and poly(styrene)-*b*-poly(methyl methacrylate) (PS-*b*-PMMA). Such a blend system combines the photodegradability of PMMA with the long-range ordering characteristics of the PEO block copolymer under solvent annealing at controlled humidity (*25*), as demonstrated by earlier work on PEO-*b*-PMMA-*b*-PS triblock copolymers (*26*). The respective PS segments were modified with small fractions of randomly incorporated 4-hydroxystyrene and 4-vinylpyridine units (*26*). Diblock copolymers of poly(ethylene oxide)-*b*-poly(styrene-*r*-4-hydroxystyrene) [PEO-*b*-P(S-*r*-4HS), denoted as A-B] and poly(styrene-*r*-4-vinylpyridine)-*b*-poly(methyl methacrylate) [P(S-*r*-4VP)-*b*-PMMA), denoted as B´-C] (Fig. 1) with B and B´ blocks as the majority segments in each copolymer were prepared using controlled free-radical polymerizations (for synthesis and characterization, see figs. S1 to S5). This allows the molecular weight of each block to be accurately controlled and the level of incorporation of the H-bonding units to be tailored by simple random copolymerization. A

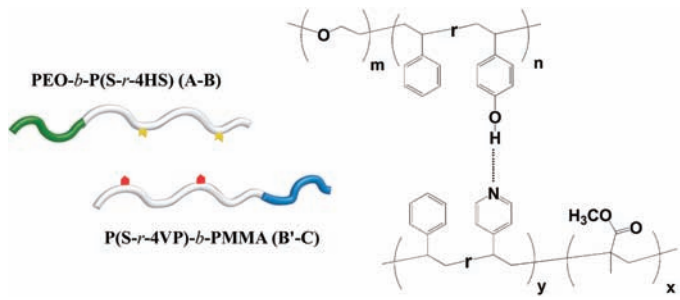

Fig. 1. Hierarchical self-assembly and target morphology for a blend of supramolecular A-B and B´-C diblock copolymers stabilized by H-bonding.

Table 1. Molecular weight and compositions of A-B and B´-C block copolymers (the last digit of each sample name denotes the average number of H-bonding units per chain). DP is the degree of polymerization for each of the components.

PEO-*b*-P(S-*r*-4HS)	DP_{EO}:DP_S:DP_{4HS}	f_{PEO} (wt %)	f_{PS} (wt %)	f_{P4HS} (wt %)
1) A-B_7	113:147:7	23.8	72.4	3.8
P(S-*r*-4VP)-*b*-PMMA	**DP_{MMA}:DP_S:DP_{4VP}**	**f_{PMMA} (wt %)**	**f_{PS} (wt %)**	**f_{P4VP} (wt %)**
2a) B´-C_6	120:220:6	33.7	64.4	1.9
2b) B´-C_8	120:195:8	36.3	61.3	2.4
2c) B´-C_14	120:188:14	36.4	59.1	4.5
2d) B´-C_25	120:219:25	32.1	61.0	6.9

[1]Materials Research Laboratory, University of California, Santa Barbara, CA 93106, USA. [2]Department of Chemical Engineering, University of California, Santa Barbara, CA 93106, USA. [3]Department of Materials, University of California, Santa Barbara, CA 93106, USA. [4]Department of Chemistry and Biochemistry, University of California, Santa Barbara, CA 93106, USA.

*To whom correspondence should be addressed. E-mail: hawker@mrl.ucsb.edu (C.J.H.); edkramer@mrl.ucsb.edu (E.J.K.); ghf@mrl.ucsb.edu (G.H.F.)

representative selection of diblock copolymers is shown in Table 1. Initially, the number of H-bonding units in the respective polystyrene blocks was kept low to minimize the chemical difference between the blocks while still enabling an overall attraction characterized by a negative Flory-Huggins parameter ($\chi < 0$).

Supramolecular block copolymer films, ~50 nm thick, were prepared by spin-coating polymer solutions in benzene onto silicon wafers, with the blends formulated by simply mixing the phenolic containing PEO A-B diblock, **1**, with the corresponding PMMA B′-C diblock, **2**, containing various levels of 4-vinylpyridine substitution. In these samples, a 1:1 molar ratio of A-B chains to B′-C chains was maintained and the films were solvent-annealed under saturated toluene vapor in a controlled high-humidity atmosphere (*26*, *27*). Figure 2 shows the atomic force microscopy (AFM) phase images of films from four representative blends, which indicate that the nanoscale morphology and grain size are affected by the composition of H-bonding components. For a blend of **1** with **2d** (ratio of phenolic groups to pyridyl groups is approximately 1:3.5), vertical cylinders were obtained, but little order, either hexagonal or square packing, was observed (Fig. 2D). Upon decreasing the phenolic:pyridyl ratio to 1:2, distinct square arrays were observed, although the ordering was poor (Fig. 2C). However, for blends with approximately equal numbers of phenolic and pyridyl units per chain, the corresponding thin films exhibited square arrays with a high degree of in-plane order. In the case of the blend of **1** and **2a**, an extremely high degree of ordering was observed, with grains of the square array morphology that were larger than 5 μm by 5 μm (Fig. 2A).

To confirm the critical role of supramolecular interactions in these systems, we examined control samples that did not have H-bonding interactions: blends of the parent polymers, PEO-*b*-PS/PS-*b*-PMMA, and blends where the phenolic unit was exchanged for an acetoxy group, PEO-*b*-P(S-*r*-4AS)/P(S-*r*-4VP)-*b*-PMMA. In each case, blends prepared using the same solvent-annealing procedure showed macrophase-separated structures with no long-range order (fig. S6). In the case of PEO-*b*-P(S-*r*-4AS)/P(S-*r*-4VP)-*b*-PMMA, we found small regions with nanoscale morphology; however, these showed hexagonal local order. The lack of uniform microphase-separated structures in these systems is not surprising and is consistent with previous studies of diblock copolymer blends (*19*–*22*). These control experiments demonstrate the critical role of supramolecular interactions in producing both long-range order and novel square arrays of nanoscale features.

The presence of square arrays of features for the blend of **1** and **2a** with near-stoichiometric numbers of H-bonding units was confirmed by a series of studies. The film-substrate interface was examined by etching the underlying oxide and lifting the polymer film off the substrate, followed by flipping and imaging by AFM (figs. S7 and S8). We observed square arrays of features with similar periodicity for the substrate interface, which suggests a perpendicular cylindrical structure spanning the entire thickness of a film. Transmission electron microscopy (TEM) images of the solvent-annealed films (Fig. 3) confirmed the square array of cylinders. A highly ordered square lattice was observed with distinct contrast between bright features, gray features, and a dark matrix (no stain was used). Further observation of the films revealed that each gray domain is surrounded by four white domains and vice versa. The dark, continuous regions are presumably PS, whereas the PMMA domains (which undergo degradation under electron beam irradiation, leading to enhanced Z-contrast with the matrix) appear white when compared to the gray regions, which correspond to PEO domains. The center-to-center spacing of the square arrays corresponds to 51 nm, which is in very good agreement with the AFM measurements.

We used numerical self-consistent field theory (SCFT) (*28*) to examine the stability of tetragonal cylinder packing in this system. In previous studies of symmetrical (bulk) ABC triblock copolymers, square lattices were experimentally observed by Mogi *et al*. (*29*, *30*) and the energetic preference of square over hexagonal cylinder packing was theoretically verified using SCFT (*31*). Applying similar methods, we examined a model A-B/B′-C diblock copolymer blend in which the supramolecular interactions are described by a simple (nonspecific) contact attraction between B and B′ segments. The diblocks were assumed to be 70% B (or B′) by volume and of equal overall molecular weight. The products of the chain length N and the segmental Flory interaction parameters were fixed at $\chi_{AB}N = \chi_{AB'}N = \chi_{B'C}N = \chi_{BC}N = 14$, $\chi_{BB'}N = -3.5$, and $\chi_{AC}N = 55$. Earlier studies indicated that during solvent annealing under high-humidity conditions, water absorption into the PEO domains increases the effective χ between PEO and PMMA segments, hence the relatively large value of $\chi_{AC}N$ used in the model (*27*, *32*). Large-cell SCFT simulations of this model launched from random initial conditions revealed no evidence of macrophase separation or hexagonal cylinder packings. In all cases, microphase-separated morphologies with well-ordered square lattices of A and C cylinders were obtained.

Figure 4 shows the microdomain structure and density plots from such a simulation. The A and C blocks (red and black) form cylinders with coronas of B and B′ (yellow and blue), respectively. The green polymer matrix reflects regions where the yellow B and blue B′ blocks are intermixed. Similar to ABC triblock copolymers, unit-cell simulations reveal that square-packed cylinders in the A-B/B′-C system have a lower free energy density than do hexagonally packed cylinders, which constitute the stable phase in simple AB diblock copolymers. In ABC triblock copolymers, the square lattice allows for a more uniform distribution of the C domains around each A domain (and vice versa), which lessens the stretching penalty of the B blocks despite not providing an optimal close packing of cylinders

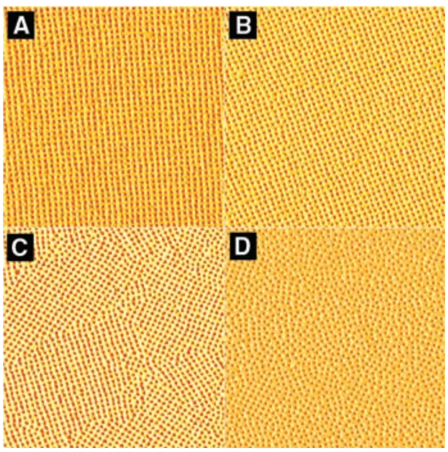

Fig. 2. AFM phase images of solvent-annealed films from blends of supramolecular block copolymers: (**A**) **1** and **2a**; (**B**) **1** and **2b**; (**C**) **1** and **2c**; (**D**) **1** and **2d**. Image sizes, 2 μm by 2 μm.

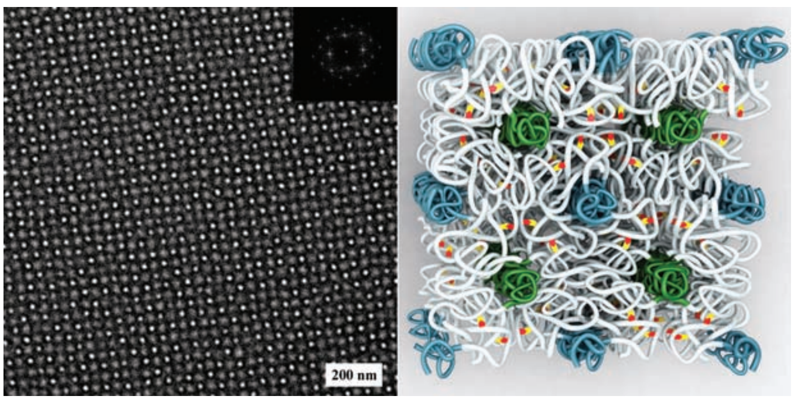

Fig. 3. TEM image and associated Fourier transform (**inset**) of a solvent-annealed blend film of supramolecular block copolymers **1** and **2a**. A cartoon (right panel) illustrates proposed chain packings.

(*31*). Although the A and C blocks do not connect on the same chain in the present blend system, favorable supramolecular interactions between B and B′ blocks mimic triblock-like behavior by encouraging B-B′ segmental mixing at relatively uniform B and B′ block extensions.

Additional evidence for the nanoscale morphology of these self-assembled films was obtained by using these materials as lithographic masks to transfer the template image into the underlying silicon substrate. A schematic route to fabricating square arrays of holes in silicon oxide from a supramolecular block copolymer film is shown in Fig. 5. The film is first irradiated with deep-UV light to degrade the PMMA domains and cross-link the PS matrix. The UV-degraded films served as masks for reactive ion etching (RIE) using CHF_3 to etch the silicon oxide; the remaining organic material was removed by O_2 plasma. Scanning electron microscope (SEM) images are also shown in Fig. 5. In the top-view SEM micrograph, the cylindrical pores from the UV-degraded regions appear darker and have a diameter of ~22 nm. The period of the holes is 50 nm, which is consistent with the AFM results for the nondegraded thin films and demonstrates a high degree of fidelity in the pattern transfer process. Of particular note is the retention of the corresponding features due to the co-registered PEO domains, which lead to small "dimples" due to the topological and etch rate differences between the PEO domains and the polystyrene matrix. Additional confirmation of the formation of cylindrical pores was obtained from the 75° cross-section images, which clearly show the formation of holes with depths of 15 to 20 nm.

By combining supramolecular assembly of H-bonding phenolic and pyridyl units with controlled microphase separation of well-defined diblock copolymers, we have shown that near-stoichiometric ratios of the H-bonding groups are critical for achieving good order as well as controlling the local packing of cylindrical domains. Degradation of the PMMA domains and subsequent etching allowed nanoscale features to be lithographically transferred with high fidelity, leading to highly ordered square arrays of ~20-nm cylindrical pores.

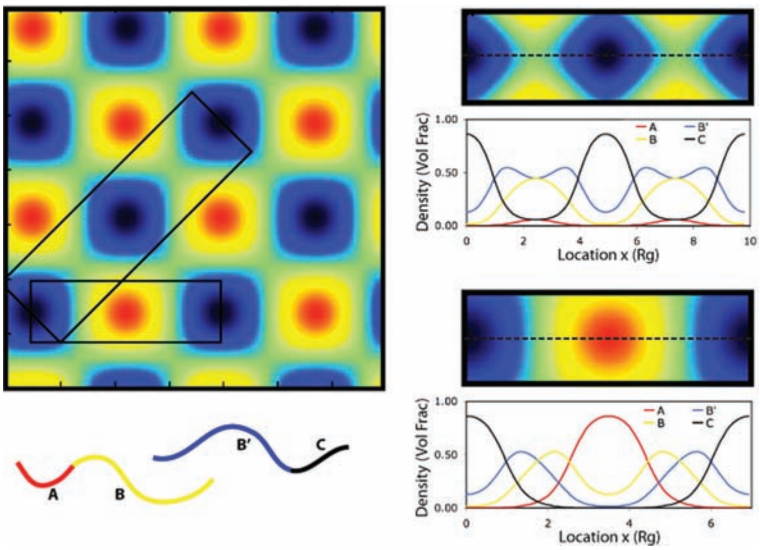

Fig. 4. SCFT simulated morphology and density profiles of an A-B/B′-C diblock copolymer blend. Regions of high A, B, B′ and C density are colored red, yellow, blue, and black, respectively. The green regions represent mixed B and B′. The boxed regions are reproduced at right, with line density profiles taken along the dashed lines.

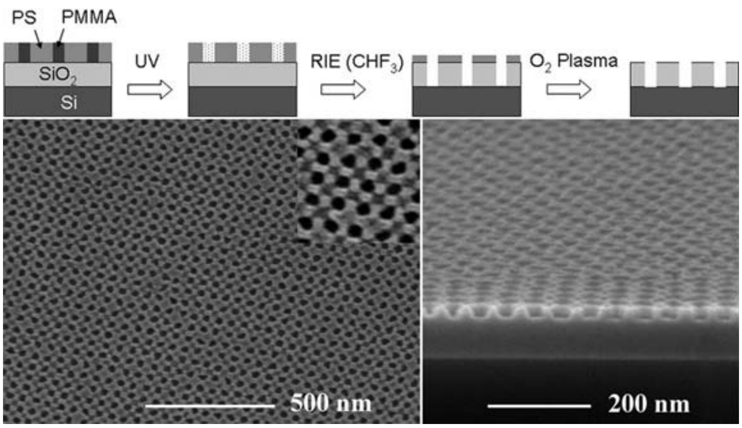

Fig. 5. (**Top**) Schematic representation of pattern transfer from supramolecular block copolymer thin films; PEO domains are omitted for clarity. (**Bottom**) SEM top view and 75° cross-section images of square arrays of cylindrical pores in silicon oxide after RIE and O_2 plasma treatment of a UV-degraded thin-film blend of supramolecular block copolymers **1** and **2a**. (Inset) Magnified SEM top view.

References and Notes

1. C. T. Black *et al.*, *Appl. Phys. Lett.* **79**, 409 (2001).
2. T. Skotnicki, J. A. Hutchby, T. J. King, H. S. P. Wong, F. Beouff, *IEEE Circuits Devices Mag.* **21**, 16 (2005).
3. M. Park, C. Harrison, P. M. Chaikin, R. A. Register, D. H. Adamson, *Science* **276**, 1401 (1997).
4. S. O. Kim *et al.*, *Nature* **424**, 411 (2003).
5. D. Y. Ryu, K. Shin, E. Drockenmuller, C. J. Hawker, T. P. Russell, *Science* **308**, 236 (2005).
6. P. Mansky, Y. Liu, E. Huang, T. P. Russell, C. J. Hawker, *Science* **275**, 1458 (1997).
7. R. A. Segalman, H. Yokoyama, E. J. Kramer, *Adv. Mater.* **13**, 1152 (2001).
8. J. Y. Cheng, C. A. Ross, E. L. Thomas, H. I. Smith, G. J. Vancso, *Appl. Phys. Lett.* **81**, 3657 (2002).
9. S. Hamm, *BusinessWeek Online*, www.businessweek.com/technology/content/may2007/tc20070502_768360.htm?chan=top+news_top+news+index_businessweek+exclusives.
10. International Technology Roadmap for Semiconductors, ITRS 2007 Edition (www.itrs.net/Links/2007ITRS/2007_Chapters/2007_ERM.pdf), pp. 22–26.
11. Square arrays are a major goal because of the considerable investment by the semiconductor industry in circuit design software, fabrication processes, etc., all based on a rectilinear coordinate system. A hexagonal pattern of vias, for example, would require extensive and very expensive reworking of the design software and fabrication protocols, whereas a square array would not. As a result, the Semiconductor Industry Association several years ago posed a challenge to researchers in block copolymer lithography to develop square arrays of etchable block copolymer domain patterns (see www.itrs.net/Links/2007ITRS/LinkedFiles/ERM/DSAR11%20082107.DOC).
12. R. A. Segalman, *Mater. Sci. Eng. Rep.* **R48**, 191 (2005).
13. J. Y. Cheng, C. A. Ross, H. I. Smith, E. L. Thomas, *Adv. Mater.* **18**, 2505 (2006).
14. S.-M. Park, G. S. W. Craig, Y.-H. La, H. H. Solak, P. F. Nealey, *Macromolecules* **40**, 5084 (2007).
15. V. Abetz, T. Goldacker, *Macromol. Rapid Commun.* **21**, 16 (2000).
16. N. Y. Vaidya, C. D. Han, *Macromolecules* **33**, 3009 (2000).
17. H. Mao, P. L. Arrechea, T. S. Bailey, B. J. S. Johnson, M. A. Hillmyer, *Faraday Discuss.* **128**, 149 (2005).
18. T. Asari, S. Matsuo, A. Takano, Y. Matsushita, *Macromolecules* **38**, 8811 (2005).
19. P. D. Olmsted, I. W. Hamley, *Europhys. Lett.* **45**, 83 (1999).
20. H. Frielinghaus *et al.*, *Macromolecules* **34**, 4907 (2001).
21. K. Kimishima, H. Jinnai, T. Hashimoto, *Macromolecules* **32**, 2585 (1999).
22. H. G. Jeon, S. D. Hudson, H. Ishida, S. D. Smith, *Macromolecules* **32**, 1803 (1999).
23. O. Ikkala, G. ten Brinke, *Chem. Commun.* **2004**, 2131 (2004).
24. R. Hoogenboom, D. Fournier, U. S. Schubert, *Chem. Commun.* **2008**, 155 (2008).
25. S. H. Kim, M. J. Misner, T. Xu, M. Kimura, T. P. Russell, *Adv. Mater.* **16**, 226 (2004).
26. J. Bang *et al.*, *J. Am. Chem. Soc.* **128**, 7622 (2006).
27. C. Tang *et al.*, *Macromolecules* **41**, 4328 (2008).

28. The SCFT simulations were run using a pseudo-spectral method with 256^2 spatial collocation points, periodic boundary conditions, and a spatial resolution of 0.05 Rg (radius of gyration) in the *x* and *y* directions. As we are primarily interested in the packing of cylinders, uniformity is assumed in the *z* direction. The free energy per chain was minimized with respect to the box size. The chains were modeled as continuous Gaussian threads and were discretized using 200 contour steps.
29. Y. Mogi *et al.*, *Macromolecules* **25**, 5408 (1992).
30. Y. Mogi *et al.*, *Macromolecules* **27**, 6755 (1994).
31. M. W. Matsen, *J. Chem. Phys.* **108**, 785 (1998).
32. J. Bang *et al.*, *Macromolecules* **40**, 7019 (2007).
33. We thank E. Pressly and M. Dimitriou for synthesis assistance. Supported by the Nanoelectronics Research Initiative under contract RID#1549 (SRC/NRI), the Focus Center Research Program (FCRP) Center on Functional Engineered Nano Architectonics, and NSF under the Materials Research Science and Engineering Center program (UCSB MRL, DMR-0520415).

Supporting Online Material
www.sciencemag.org/cgi/content/full/1162950/DC1
Materials and Methods
Figs. S1 to S8
References

8 July 2008; accepted 5 September 2008
Published online 25 September 2008;
10.1126/science.1162950
Include this information when citing this paper.

The Extreme Kuiper Belt Binary 2001 QW$_{322}$

J.-M. Petit,[1,3]* J. J. Kavelaars,[2] B. J. Gladman,[3] J. L. Margot,[4] P. D. Nicholson,[4] R. L. Jones,[5] J. Wm. Parker,[6] M. L. N. Ashby,[7] A. Campo Bagatin,[8] P. Benavidez,[8] J. Coffey,[3] P. Rousselot,[1] O. Mousis,[1] P. A. Taylor[4]

The study of binary Kuiper Belt objects helps to probe the dynamic conditions present during planet formation in the solar system. We report on the mutual-orbit determination of 2001 QW$_{322}$, a Kuiper Belt binary with a very large separation whose properties challenge binary-formation and -evolution theories. Six years of tracking indicate that the binary's mutual-orbit period is ≈25 to 30 years, that the orbit pole is retrograde and inclined 50° to 62° from the ecliptic plane, and, most surprisingly, that the mutual orbital eccentricity is <0.4. The semimajor axis of 105,000 to 135,000 kilometers is 10 times that of other near-equal-mass binaries. Because this weakly bound binary is prone to orbital disruption by interlopers, its lifetime in its present state is probably less than 1 billion years.

A combination of survey strategies and adaptive optics technologies has led to a surge in the discovery rate of binary minor planets. Since 2001, newly discovered binaries in the main asteroid and Kuiper Belts have been announced at the rate of about seven per year (*1*, *2*). There are now more than 100 known binaries, nearly half of which are Kuiper Belt objects (KBOs). Measurements of the frequency of binary objects and their sizes and orbital configurations constrain their formation and evolution mechanisms, theories of planetesimal accretion and disruption, and the collisional history of the Kuiper Belt.

Discovering and studying the mutual orbits of binary systems is currently the only way to directly determine KBO masses. Assuming that the optical properties of the KBO binaries are representative of the whole KBO population, one can link mass to apparent magnitude and hence estimate the total mass of the Kuiper Belt without requiring assumptions on albedo and density. Recent Hubble Space Telescope observations (*3*) indicate that KBOs display a wide range of albedos (8 to 40%, assuming unit density), which complicate the estimation of the total mass of the Kuiper Belt using a luminosity function. Combined with thermal infrared observations, phase-function photometry, or star occultation observations, direct determination of KBO masses leads to the determination of their density and bulk composition.

Here we report the mutual-orbit determination of the large-separation Kuiper Belt binary, 2001 QW$_{322}$ (*4*). This KBO was discovered in data acquired on 24 August 2001 at the Canada-France-Hawaii Telescope by the Canada-France Ecliptic Plane Survey team. The two components had identical magnitudes of $m_R \simeq 24.0$ within the measurement uncertainties, implying essentially equal sizes. Only one other equal-component binary was known at the time, asteroid (90) Antiope, with a magnitude difference of ~0.1 mag (*5*). However, 2001 QW$_{322}$ was obviously exceptional because the measured separation of ~4″ at its distance of 43 astronomical units (AU) corresponds to a sky-projected physical separation of 125,000 km (about one-third of the distance from Earth to the Moon), far larger than any other small-body binary.

The large separation implied a mutual-orbit period of at least several years. Six years of tracking with the use of 4- to 8-m class telescopes (Fig. 1) resolved that 2001 QW$_{322}$, an object in the main classical Kuiper Belt (*6*), has a low-eccentricity mutual orbit with a separation of 105,000 to 135,000 km, greater than any other

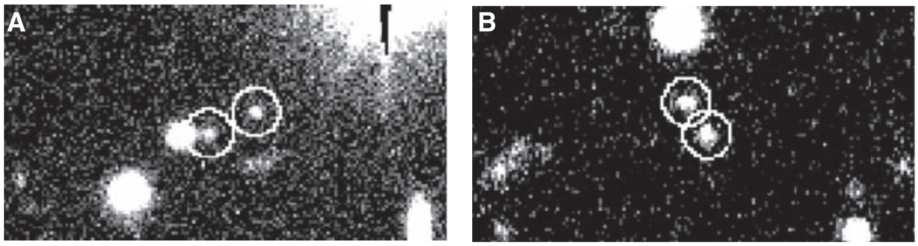

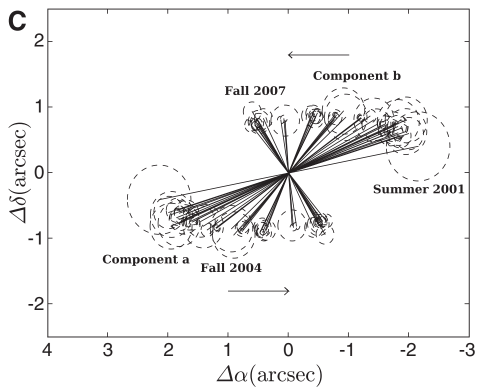

Fig. 1. (**A**) Image of the Kuiper Belt binary 2001 QW$_{322}$ from VLT on 3 September 2002. The separation between the two components at the time was 3.4″. (**B**) Image from Gemini-South on 17 September 2007; the separation was 1.8″. In both panels, the components are circled; in all panels, north is up and east is to the left. The "a" component is the most southern one. (**C**) Relative position of the two components of 2001 QW$_{322}$. The origin corresponds to the center of mass, assuming equal mass for both components. The southern "a" component has been moving westward, whereas the northern "b" component has been moving to the east. $\Delta\alpha$, the separation between components in right-ascension; $\Delta\delta$, the separation of declination.

[1]Observatoire de Besançon, Universite de Franche Comte, Besancon, Doubs 25010, France. [2]Herzberg Institute of Astrophysics, National Research Council, Victoria, BC V9E 2E7, Canada. [3]Department of Physics and Astronomy, University of British Columbia, Vancouver, BC V6T 1Z1, Canada. [4]Department of Astronomy, Cornell University, Ithaca, NY 14853, USA. [5]Department of Astronomy, University of Washington, Seattle, WA 98195–1580, USA. [6]Southwest Research Institute, Boulder, CO 80302–5150, USA. [7]Harvard-Smithsonian Center for Astrophysics, Cambridge, MA 02138, USA. [8]Escuela Politecnica Superior, University of Alicante, Alicante 03080, Spain.

*To whom correspondence should be addressed. E-mail: petit@obs-besancon.fr